Stability and acoustic scattering in a cylindrical thin shell containing compressible mean flow

E. J. BRAMBLEY AND N. PEAKE

Department of Applied Mathematics and Theoretical Physics, University of Cambridge, Centre for
Mathematical Sciences, Wilberforce Road, Cambridge CB3 0WA, UK

We consider the stability of small perturbations to a uniform inviscid compressible flow within a cylindrical linear-elastic thin shell. The thin shell is modelled using Flügge's equations, and is forced from the inside by the fluid, and from the outside by damping and spring forces. In addition to acoustic waves within the fluid, the system supports surface waves, which are strongly coupled to the thin shell. Stability is analysed using the Briggs–Bers criterion, and the system is found to be either stable or absolutely unstable, with absolute instability occurring for sufficiently small shell thicknesses. This is significantly different from the stability of a thin shell containing incompressible fluid, even for parameters for which the fluid would otherwise be expected to behave incompressibly (for example, water within a steel thin shell). Asymptotic expressions are derived for the shell thickness separating stable and unstable behaviour.

We then consider the scattering of waves by a sudden change in the duct boundary from rigid to thin shell, using the Wiener–Hopf technique. For the scattering of an inbound acoustic wave in the rigid-wall section, the surface waves are found to play an important role close to the sudden boundary change. The solution is given analytically as a sum of duct modes.

The results in this paper add to the understanding of the stability of surface waves in models of acoustic linings in aeroengine ducts. The oft-used mass–spring–damper model is regularized by the shell bending terms, and even when these terms are very small, the stability and scattering results are quite different from what has been claimed for the mass–spring–damper model. The scattering results derived here are exact, unique and causal, without the need to apply a Kutta-like condition or to include an instability wave. A movie is available with the online version of the paper.

1. Introduction

In this paper, we consider a cylindrical thin shell within which flows a compressible inviscid fluid. The fluid flow is axial, uniform, steady, and subsonic. To this situation we introduce small unsteady perturbations, and consider their nature, stability, and scattering properties. From an acoustics perspective, this is the study of the acoustics of a cylindrical thin shell waveguide with mean flow. From a fluid-loaded structures perspective, it is the study of a fluid-loaded linear-elastic cylindrical thin-shell, where the fluid is compressible and has a significant mean flow; the degree of fluid loading is arbitrary, and may be heavy (e.g. water within a steel cylinder) or light (e.g. air within an aluminium cylinder).

The response of a fluid-loaded cylindrical thin shell has been much studied, although mostly with incompressible fluid and zero mean flow. Crighton & Oswell (1991) pointed out that, for a fluid-loaded flat plate, the inclusion of mean flow significantly modifies the problem, and can cause a change in stability, because the mean flow provides an energy reservoir that can feed the small perturbations and give rise to instabilities, analogous to the Kelvin–Helmholtz shear layer instability. Crighton & Oswell's analysis was extended to a fluid-loaded cylindrical thin shell by Peake (1997), and the curvature of the thin shell was found to have a dramatic effect on stability. Here, we extend Peake's analysis to account for a compressible mean flow.

Acoustic modes in a straight cylindrical duct with rigid walls and mean flow are very well understood, with the only effect of the mean flow being to introduce a Doppler shift. The interesting question is in the model of the boundary, and particularly the ability of the boundary to attenuate sound. For a mass–spring–damper boundary model, Rienstra (2003) discovered that as well as modifying the wavenumbers of the acoustic duct modes, the boundary model gave rise to an extra set of modes without rigid-wall counterparts. Rienstra termed these *surface modes*, since they tend to be localized about the duct boundary. The surface modes have a distinctly different character from the acoustic modes, and have deep connections with the boundary model and stability; indeed, Rienstra tentatively identified one surface wave as an instability. Described in cylindrical polar coordinates (r, θ, x), the duct boundary is characterized by its impedance $Z = p/v$, where a fluid pressure $p \exp\{i\omega t - ikx - im\theta\}$ at the boundary produces a radial boundary velocity $v \exp\{\cdots\}$. The mass–spring–damper model (effectively a modified Winkler foundation) assumes the radial boundary displacement w to be governed by

$$d\frac{\partial^2 w}{\partial t^2} + R\frac{\partial w}{\partial t} + bw = p. \tag{1.1}$$

This leads to the impedance $Z = R + id\omega - ib/\omega$. The lack of x and θ derivatives in this boundary model cause Z to be independent of both k and m, and corresponds to the assumption that the boundary is infinitely flexible and locally reacting. Here, we extend this expression for Z to include wavenumber-dependent terms arising from the elastic behaviour of a cylindrical shell.

There are various methods by which stability may be analysed. The choice of method seems moderately controversial, and so warrants some discussion. A commonly used and proven stability analysis is the Briggs–Bers criterion (Briggs 1964; Bers 1983), which was used by Crighton & Oswell (1991) and Peake (1997). This criterion is only applicable provided $\text{Im}(\omega(k))$ is bounded below for real k†, or in other words, provided the temporal growth rate of the system is bounded for any initial conditions. Unfortunately, the mass–spring–damper boundary model turns out to belong to a class of problems, also including the Kelvin–Helmholtz vortex sheet instability, for which this is not the case, and so the Briggs–Bers criterion is inapplicable. Various authors have considered the stability of this class of systems. Jones & Morgan (1972) analysed the stability of a vortex sheet, and derived an explicit causal solution in terms of ultradistributions. In a later paper, Jones & Morgan (1974, p. 25) formalized this derivation into a stability criterion, which was extensively used

† By $\omega(k)$, we mean the multi-valued function giving the frequencies of all modes for a specified k; i.e. all allowable values of ω for solutions of the form $f(r, \theta)\exp\{i\omega t - ikx\}$ for a given k. See figure 2 for an example. Note that we use the opposite sign convention for the time Fourier transform to Briggs.
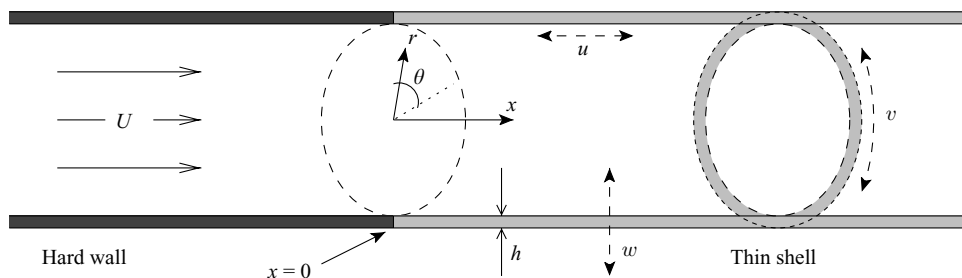
FIGURE 1. Schematic of a cylindrical duct with a sudden change from rigid-wall boundary for $x < 0$ to thin-shell boundary for $x > 0$. The small unsteady perturbations to the position of the thin shell are given by u, v, and w.

at the time (e.g. Morgan 1975; Munt 1977). Crighton & Leppington (1974) considered a semi-infinite plate shedding a vortex sheet. They proposed (Crighton & Leppington 1974, p. 406), although left unproven, a stability criterion similar to Briggs–Bers, for use in similar problems to their own. They went on to derive an explicit causal solution in terms of ultradistributions, in a similar manner to Jones & Morgan (1972).

The stability of the vortex sheet problems was also investigated by Jones (1977), who regularized the problem by considering a shear layer of finite thickness H. Jones concluded that for H small but non-zero an instability was present that could be represented in terms of conventional functions, which in the limit $H \to 0$ yielded the previously known ultradistribution result. For the problem considered here of an externally damped cylindrical thin shell of thickness h bounding compressible mean flow, the temporal growth rate is bounded, and so the Briggs–Bers criterion is used to analyse stability, while the mass–spring–damper boundary is recovered in the limit of vanishing shell thickness, $h \to 0$. This may be used to better understand the stability of the mass–spring–damper boundary model.

Rienstra (2007) recently analysed the scattering of a downstream-propagating rigid-wall acoustic mode as it encounters a sudden transition at $x = 0$ to a locally reacting lined duct, using the Wiener–Hopf technique. Owing to the uncertainty over whether one of the surface modes represents an instability or not, both cases were considered. Assuming all modes to be stable, the surface streamline was found to be $O(x^{1/2})$ as $x \to 0$, giving a cusp in the boundary at $x = 0$. Treating one surface mode as an instability, an extra degree of freedom became available which can be chosen to satisfy a Kutta-like condition, giving the surface streamline behaviour as $O(x^{3/2})$ at the boundary transition. Using the thin-shell boundary model, it is found that the surface streamline is $O(x^2)$ across the boundary transition, with no instabilities present and without the need to appeal to a Kutta-like condition.

2. Governing equations and the dispersion relation

A straight cylindrical duct of radius r_0 and of infinite extent in the x-direction is considered, as shown in figure 1. An inviscid steady uniform axial flow of speed U, density D, pressure P, and sound speed C flows down the inside of the duct in the positive x-direction. Speeds are non-dimensionalized by the speed of sound C, so that U becomes the (subsonic) mean flow Mach number. Distances are non-dimensionalized by the duct radius r_0, times by r_0/C, densities by D, and pressures by DC^2. (Note that for a perfect gas with ratio of specific heats γ, this gives the mean non-dimensionalized pressure as $1/\gamma$).

A small potential perturbation $\phi(x, r, \theta, t)$ to the steady state is considered, with corresponding velocity perturbation $\boldsymbol{u} = \nabla\phi$, pressure p and density ρ. The linearized governing equations given by Goldstein (1978) in this case become

$$\frac{\mathrm{D}^2\phi}{\mathrm{D}t^2} - \nabla^2\phi = 0 \quad \text{and} \quad p = \rho = -\frac{\mathrm{D}\phi}{\mathrm{D}t},$$

where $\mathrm{D}/\mathrm{D}t = \partial/\partial t + U\partial/\partial x$ is the convective derivative with respect to the mean flow. Using separation of variables, a solution of the form $\phi = f(r)\exp\{\mathrm{i}\omega t - \mathrm{i}kx - \mathrm{i}m\theta\}$ is sought. With the non-dimensionalization above, ω is the Helmholtz number, k is the *axial wavenumber*, and m (an integer) is the *azimuthal wavenumber*. Making this substitution, and requiring the solution to be non-singular at $r = 0$, gives $f(r) = A\mathrm{J}_m(\alpha r)$ for some constant amplitude A, where J_m is the mth Bessel function of the first kind and $\alpha^2 = (\omega - Uk)^2 - k^2$.

The duct boundary is modelled as a flexible impermeable surface with radius $1 + w$, where w is the small unsteady perturbation. The motion of the boundary complicates the no-flux boundary condition $\boldsymbol{u}\cdot\hat{\boldsymbol{n}} = 0$ applied on the surface, since both the position of the surface and the direction of the surface normal $\hat{\boldsymbol{n}}$ are unsteady and dependent on the flow. For a general geometry, Myers (1980) derived the linearized no-flux boundary condition to be

$$\boldsymbol{u}\cdot\boldsymbol{n} = \left(\frac{\partial}{\partial t} + \boldsymbol{U}\cdot\nabla - (\boldsymbol{n}\cdot\nabla\boldsymbol{U})\cdot\boldsymbol{n}\right)w,$$

where $\boldsymbol{n}$ is the unperturbed surface normal out of the fluid, $\boldsymbol{U}$ is the steady mean flow, and all quantities are evaluated on the unperturbed boundary. Substituting the solution for ϕ into this, and using $p/w = \mathrm{i}\omega Z$, yields the dispersion relation

$$1 - \frac{(\omega - Uk)^2}{\mathrm{i}\omega Z}\frac{\mathrm{J}_m(\alpha)}{\alpha\mathrm{J}'_m(\alpha)} = 0. \tag{2.1}$$

Note that since $\mathrm{J}_m(-r) = (-1)^m\mathrm{J}_m(r)$, (2.1) is a meromorphic function of α^2 and contains no branch cuts, and so it does not matter which branch is chosen for α. The dispersion relation for a rigid wall is obtained by taking $Z \to \infty$ to give $\mathrm{J}'_m(\alpha) = 0$. The key question now is: what is an appropriate function for $Z(\omega, k, m)$?

2.1. *Impedance of a thin-shell boundary*

The duct boundary is modelled as the interior of a thin cylindrical shell using Flügge's equations (see Païdoussis 2004, p. 576), the outside of which is sprung and damped. Let u, v, and w denote the axial, azimuthal, and radial displacement of the shell from equilibrium, as shown in figure 1, and let $p^* = p - bw - R\partial w/\partial t$ be the net outward force per unit area on the shell. Here, p is the linearized acoustic pressure in the fluid at the duct boundary, and b and R represent a spring force and damping respectively, assumed to originate from the outside of the shell. All variables p, u, v, and w are taken to have $\exp\{\mathrm{i}\omega t - \mathrm{i}kx - \mathrm{i}m\theta\}$ dependence, and the impedance $Z(\omega, k, m)$ is sought, where $Z = p/(\partial w/\partial t)$. We assume that the thin-shell thickness $h \ll 1$, which simplifies Flügge's equations to those of Vlasov (see Leissa 1973, pp. 32–34). Additionally, we assume that that $2m^2 - 1 \ll (k^2 + m^2)^2$, which is almost always true† and simplifies the equations further (eliminating the diagonal term from Vlasov's

---

† It is true provided $|m| \neq 0, 1, 2$, or if otherwise provided k is sufficiently far from the origin (say $|k| \geqslant 3$). This will be seen to be very unrestrictive: typically, $m \in [0, 24]$ and $|k| \in [0, 80]$.

thin-shell equation (2.9g), Leissa 1973). The Fourier-transforms of these equations then give

$$Z = R - \mathrm{i}(c_l^2 d + b)/\omega + \mathrm{i}d\omega - \frac{\mathrm{i}c_l^2 d}{\omega} \left(\frac{h^2}{12}(k^2 + m^2)^2 - A_1 \frac{\mathrm{i}u}{w} - A_2 \frac{\mathrm{i}v}{w} \right), \qquad (2.2a)$$

where

$$\begin{pmatrix} a_{11} & a_{12} \\ a_{12} & a_{22} \end{pmatrix} \begin{pmatrix} \mathrm{i}u/w \\ \mathrm{i}v/w \end{pmatrix} = \begin{pmatrix} A_1 \\ A_2 \end{pmatrix}, \qquad (2.2b)$$

$$a_{11} = k^2 + \frac{1-\nu}{2}m^2 - \frac{\omega^2}{c_l^2}, \quad a_{12} = \frac{1+\nu}{2}mk, \quad a_{22} = m^2 + \frac{1-\nu}{2}k^2 - \frac{\omega^2}{c_l^2},$$

$$A_1 = k \left[\nu + \frac{h^2}{12} \left(k^2 - \frac{1-\nu}{2}m^2 \right) \right], \quad A_2 = m \left[1 + \frac{h^2}{12} \frac{3-\nu}{2}k^2 \right], \qquad (2.2c)$$

and $c_l^2 = E/(\rho_s(1-\nu^2))$ is the square of the speed of longitudinal compressive waves in the boundary material, $d = \rho_s h$ is the shell mass per unit area, and the properties of the boundary material ρ_s, E and ν are the density, Young's modulus, and Poisson's ratio respectively.

If k is large and $m/k \lesssim O(1)$ (of particular interest for stability analysis), and the determinant of the matrix in (2.2b) is non-zero, then $u/w = O(h^2 k)$, $v/w \lesssim O(h^2 k)$, and $A_1 u/w + A_2 v/w = O(h^4 k^4)$. Neglecting the terms involving A_1 and A_2 in (2.2a) is therefore justified in this limit, and the thin-shell impedance (2.2a) takes the form of a modified mass–spring–damper system (cf. equation (1.1)), together with a bending stiffness $B \equiv c_l^2 dh^2/12$.

The determinant of (2.2b) is zero when $k = \pm k_l$ or $k = \pm k_t$, where

$$k_l^2 = \omega^2/c_l^2 - m^2 \quad \text{and} \quad k_t^2 = \omega^2/c_t^2 - m^2 \qquad (2.3)$$

and $c_t = c_l\sqrt{(1-\nu)/2}$ is the speed of transverse waves in the duct boundary. The imaginary parts of k_l and k_t are here taken negative, or if zero the real parts are taken positive, so as to represent right-propagating longitudinal and transverse waves in the thin-shell boundary.

2.2. *Surface modes*

The main mathematical distinction between surface modes and acoustic modes is in the value of α in (2.1); acoustic modes have nearly all real α, while surface modes have a significant imaginary part to α. Rienstra (2003) derived a dispersion relation for the surface modes in the asymptotic limit $\omega \to \infty$. Recently, Brambley & Peake (2006) gave a more accurate asymptotic approximation, written in the present notation as

$$\sqrt{k^2 + m^2 - (\omega - Uk)^2} - \frac{(\omega - Uk)^2}{\mathrm{i}\omega Z} = 0, \qquad (2.4)$$

where the real part of $\sqrt{\cdots}$ is required positive. Modes which satisfy (2.4) but not this positivity condition are here termed *fake surface modes*, since they do not correspond to actual roots of the full dispersion relation (2.1).

For a locally reacting boundary (such as the mass–spring–damper boundary in equation (1.1)), Z is independent of k, and (2.4) may be rearranged to give a quartic equation for k. There would therefore be at most four roots for any given ω and m; the nature and position of these four surface modes has been discussed in detail by Rienstra (2003) and Brambley & Peake (2006). For the thin-shell impedance, (2.4)

may be rearranged to give an 18th-order polynomial in k for fixed ω, or a 14th-order polynomial in ω for fixed k. For a given frequency, there are therefore a maximum of 18 surface modes, although some of these may be fake surface modes. The surface modes may be prominently seen in figure 7.

From considering a large number of different parameters in different regimes and numerically calculating the axial wavenumbers, some interpretation of the nature and physical mechanisms supporting these surface modes may be speculated. Of the 18 potential surface modes, one real surface mode and one fake surface mode tend to each of k_l, k_t, $-k_l$, and $-k_t$ (defined in (2.3)) as $h \to 0$, and surface modes of this type are here termed *quasi-solid* surface modes. It should be emphasized, however, that these surface modes are distinct from the solid boundary waves with wavenumbers exactly equal to $\pm k_l$ and $\pm k_t$; the quasi-solid modes are fluid modes occurring in the vicinity of the boundary, whereas the solid boundary waves correspond to zeros of the determinant of (2.2b) and therefore produce no disturbance in the fluid. Of the remaining 10 surface modes, four fake and two real surface modes tend to infinity as $h \to 0$, while the other four tend to the mass–spring–damper values. This suggests that of the 18 potential surface modes, eight are sustained by compressional and twisting solid mechanisms, six are supported by bending solid mechanisms, and four are supported by effectively mass–spring–damper mechanisms.

If the terms involving A_1 and A_2 in (2.2a) may be neglected (recall that this is the case when k is large), (2.4) can be rearranged to give

$$(k^2 + m^2 - (\omega - Uk)^2)\big((c_l^2 d + b) + \mathrm{i}\omega R - d\omega^2 + B\,(k^2 + m^2)^2\big)^2 - (\omega - Uk)^4 = 0. \tag{2.5}$$

This is now a polynomial of 10th order in k, or of 6th order in ω. This dispersion relation has proved to be remarkably accurate for all cases we have considered, even for modest values of k for which the previous argument for neglecting A_1 and A_2 is not appropriate. However, this simplification does neglect the compressional and twisting components in the solid, and consequently the eight quasi-solid surface modes are not modelled by (2.5).

3. Stability

We now turn to the question of their stability, by employing the Briggs–Bers criterion (Briggs 1964; Bers 1983). In order for this criterion to be applicable, $\mathrm{Im}(\omega(k))$ for real k must be bounded below, which is not true for the mass–spring–damper model. We now verify that the Briggs–Bers criterion is applicable for the thin-shell model.

The acoustic modes are stable, being analogous to the stable rigid-wall duct modes, and do not therefore preclude the Briggs–Bers criterion from being applied. Utilizing (2.4), and noting from (2.2a) that $|Z| \to \infty$ as $|k| \to \infty$, two classifications of surface modes emerge in the limit $|k| \to \infty$,

$$\omega = Uk \pm \sqrt{k^2 + m^2} + O(k^{-5}),$$
$$\omega = \pm\sqrt{B/d}(k^2 + m^2 + 1/2) + \frac{\mathrm{i}}{2d}(R \pm 1) + O(k^{-1}),$$

where the two $\pm$ in the last equation are independent. Accounting for zeros of the determinant of (2.2b) gives an additional surface mode classification, consisting of
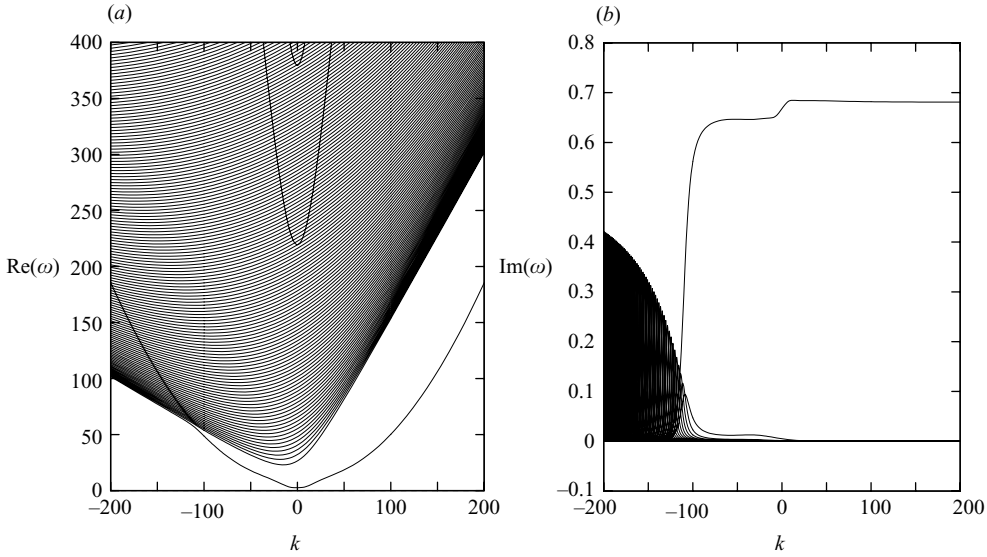
FIGURE 2. Trajectories of $\omega(k)$ for k real. For clarity, only modes with $\text{Re}(\omega) > 0$ are shown. The fluid is air and the boundary is aluminium. $h = 10^{-3}$, $U = 0.5$, $R = 3$, $b = 1$, and $m = 24$.

eight modes of the form

$$\omega = \pm c_l k + O(k^{-1}) \quad \text{or} \quad \omega = \pm c_t k + O(k^{-1}).$$

All of the above surface modes have bounded $\text{Im}(\omega)$ for real k as $|k| \to \infty$, and the regularity of (2.4) means that $\omega(k)$ is continuous, and hence bounded for k in a bounded interval. Therefore, the image of the real-k-axis in the ω-plane has bounded imaginary part, and so the Briggs–Bers criterion can be used.

The boundedness of $\text{Im}(\omega(k))$ for real k as $|k| \to \infty$ does not hold for the mass–spring–damper system. To see how this is regularized by the inclusion of bending stiffness for $h \neq 0$, set $\omega = N\sqrt{k}$ in (2.5) to find

$$N^2 = -\frac{U^2}{\beta d} + \frac{B}{d} k^3,$$

to leading order as $|k| \to \infty$, where $\beta = \sqrt{1 - U^2}$. The unbounded $\omega = -iU\sqrt{k/(\beta d)}$ behaviour found by Rienstra (2007) is therefore seen to hold only for

$$|k| \ll \left(\frac{U^2}{\beta B} \right)^{1/3}, \tag{3.1}$$

giving an estimate of the magnitude of k for which bending stiffness becomes important for stability. An example demonstrating this is given in §3.2.

3.1. *A stable example*

Figure 2 shows the real-k-axis mapped into the ω-plane for an air-filled aluminium duct, with $m = 24$, $R = 3$, and $b = 1$. The duct may be thought of as having a 1 m radius and a shell thickness of 1 mm. The many near-parallel trajectories in figure 2(*a*) correspond to members of the infinite family of acoustic modes, while the few other modes are the surface modes. Note that no modes are present with $\text{Im}(\omega) < 0$, so that the temporal inversion contour $\mathscr{C}_\omega$ may be taken arbitrarily close to the real-ω-axis.
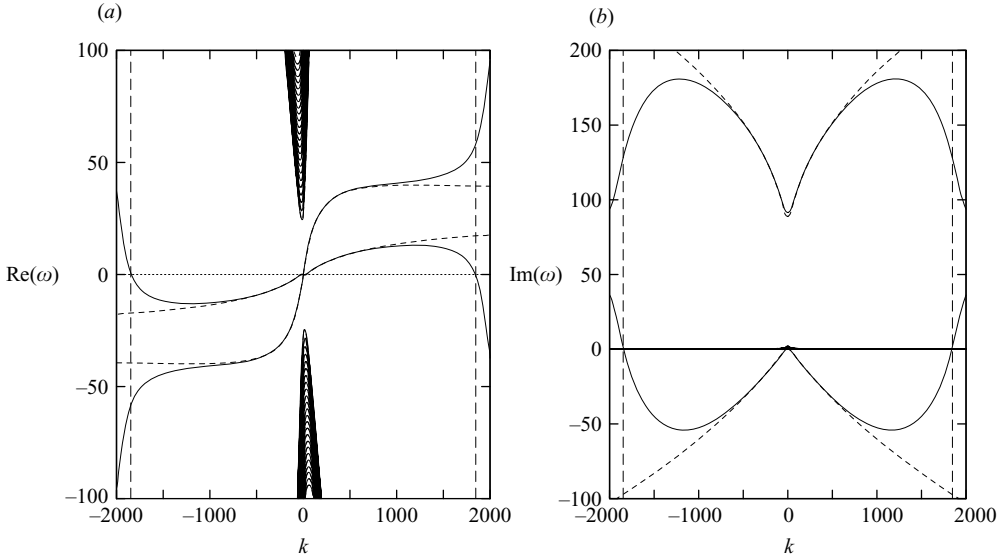
FIGURE 3. Trajectories of $\omega(k)$ for k real. Parameters are as for figure 2, but with $h = 10^{-5}$. Solid lines correspond to a thin shell, dashed lines show the equivalent mass–spring–damper trajectories. The value of k given by 3.1 is shown by the dashed vertical lines.

Hence, any mode with complex $k(\omega)$ corresponds to an exponentially decaying mode, while if $k(\omega)$ is real, the mode is left propagating if $\mathrm{Re}(c_g) < 0$, and right propagating if $\mathrm{Re}(c_g) > 0$, where $c_g = \partial\omega/\partial k$ is the group velocity, and there is no possibility of absolute instability. This is exactly as might have been naively expected without a detailed stability analysis, and shows that for these parameters the system is stable.

3.2. *An example of instability*

Using the same parameters as above, but with a very thin shell thickness $h = 10^{-5}$, leads to the situation shown in figure 3. We now investigate whether there is a pinch frequency ω_p, leading to an absolute instability. Writing the dispersion relation (2.1) as $\Delta(k, \omega) = 0$, we look for a double root, given by $\partial\Delta/\partial k = 0$. The values of ω and k which simultaneously satisfy both of these constraints were found numerically using a two-dimensional Newton–Raphson iteration, with starting points located on a grid covering the relevant areas of the k- and ω-planes. The values of ω found are shown in figure 4. The majority of these double roots involve the collision of two modes both originating from the same half of the k-plane, and so do not pinch the k-inversion contour $\mathscr{C}_k$. A double root that does pinch the contour is found to at $\omega_p = \pm 13 - 54i$, and so for these parameters the system is absolutely unstable. The extreme parameters needed to demonstrate this instability may be thought of as a 1 m duct radius with a boundary thickness of 0.01 mm and a mean flow Mach number of 0.5, which is not realizable in practice.

3.3. *The boundary between stable and unstable behaviour*

The question now arises: how small a shell thickness is needed for there to be an absolute instability? By tracking the pinch frequency numerically as h is varied, the critical value $h = h_c$ giving $\mathrm{Im}(\omega_p) = 0$ may be found. Figure 5 plots these values of h_c for a variety of parameters; the amount of external damping, R, is found to have no effect on the critical shell thickness h_c, and so figure 5 only considers $R = 3$. For
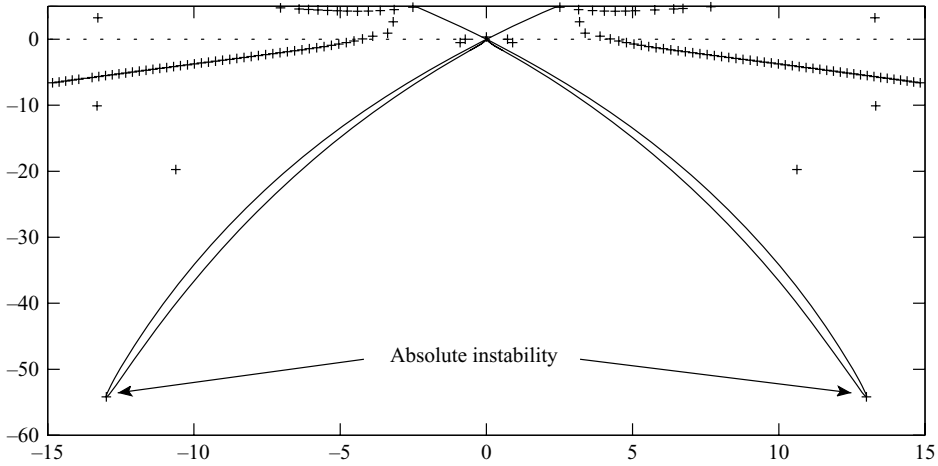
FIGURE 4. Values of ω (denoted +) for which double roots of the dispersion relation occur for some value of k. The solid line is $\omega(k)$ for real k. Parameters are as for figure 3.
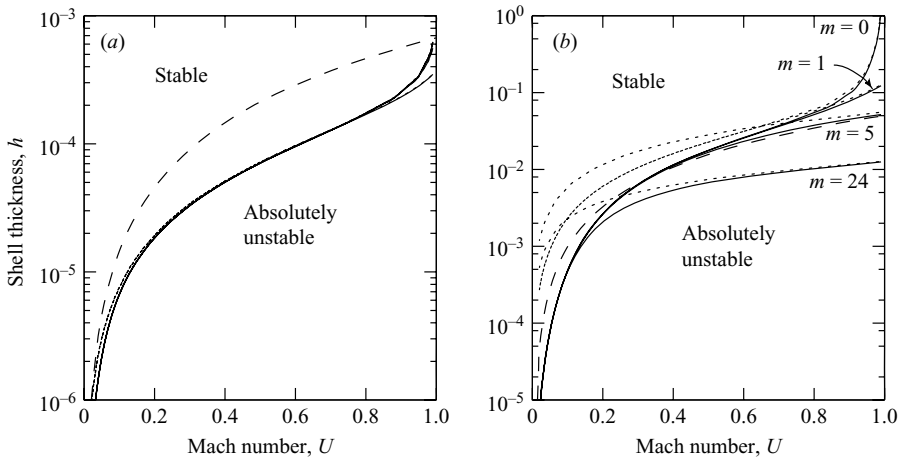

FIGURE 5. Stability for two regimes given in table 1: (a) air within aluminium and (b) water within steel. The critical shell thickness h_c is given by short dashed lines are for $b = 0$, solid lines for $b = 1$, and long dashed lines are from Peake (1997).

small U the dominant parameter is the Winkler foundation spring constant b, while as U approaches unity m becomes the dominant parameter.

The approximate critical shell thickness found by Peake (1997, equation (3.3)) is also plotted in figure 5. This result was derived for an incompressible fluid in the small-mean-flow limit, and was shown to give a very accurate approximation to the true critical boundary for an incompressible fluid. Figure 5 shows that compressibility alters the stability boundary significantly.

For a double root to correspond to a pinch, one mode must originate from the upper-half k-plane and one from the lower-half. Hence, at least one of these modes must cross the real-k-axis, shown as a solid line in figure 4 making two fingers in

Fluid	Solid	c_l	ρ_s	ν
Air	Aluminium	15.8	2 200	0.33
Water	Steel	3.6	7.85	0.3

TABLE 1. Non-dimensionalized thin-shell parameters used.

the lower-half ω-plane. As h is increased, these two fingers shrink, until at a certain value of h there are no modes with real k in the lower-half ω-plane, and so there can be no instabilities (either absolute or convective). The dominant pinch frequency ω_p is located towards the ends of these fingers, and the critical shell thickness h_c turns out to be exactly the value of h for which these fingers disappear from the lower-half ω-plane. This implies the interesting result that the system is either absolutely unstable or stable, but never only convectively unstable. Why this should be the case, rather than the pinch point crossing the boundary of one of the fingers and producing convective instability, is at present unclear. Since the two fingers of $\omega(k)$ for real k shrink down to $\omega = 0$, the critical value of ω_p, defined as $\mathrm{Im}(\omega_p) = 0$, actually occurs at $\omega_p = 0$. Using this, 2.5 tells us that this borderline is given by $\Delta = \partial\Delta/\partial k = 0$, where

$$\Delta \equiv (k^2 + m^2/\beta^2)((c_l^2 d + b)/B + (k^2 + m^2)^2)^2 - \frac{U^4 k^4}{B^2 \beta^2} \tag{3.2}$$

and $\beta^2 = 1 - U^2$. These two equations can be solved for h_c and the corresponding value of $k = k_p$. Note that the boundary damping R does not occur in (3.2), explaining why the curves in figure 5 are independent of R. However, the general solution of $\Delta = \partial\Delta/\partial k = 0$ involves solving simultaneously a 10th- and eighth-order polynomial. Progress may be made by considering the case for which $k_p \gg m/\beta$, which will turn out to be valid provided U is sufficiently small. Neglecting the terms involving m^2 in (3.2) then gives

$$\frac{1}{k_p^2}\Delta \equiv k_p^8 + 2\lambda k_p^4 - k_0^6 k_p^2 + \lambda^2 = 0,$$

$$\frac{1}{2k_p}\frac{\partial\Delta}{\partial k} \equiv 5k_p^8 + 6\lambda k_p^4 - 2k_0^6 k_p^2 + \lambda^2 = 0,$$

where $\lambda = (c_l^2 d + b)/B$, and $k_0 = (U^2/(\beta B))^{1/3}$ is the value of k given in 3.1 for which bending becomes important to stability. Solving these two equations gives

$$h_c = -\frac{b}{2c_l^2 \rho_s} + \frac{1}{2}\sqrt{\left(\frac{b}{c_l^2 \rho_s}\right)^2 + \left(\frac{9U^4}{(1 - U^2)c_l^4 \rho_s^2}\right)^{2/3}}. \tag{3.3}$$

If $U \ll 1$, this reduces to two cases, depending on whether $U \ll U_c$ or $U \gg U_c$, where

$$U_c = \left(\frac{8b^3}{9c_l^2 \rho_s}\right)^{1/4}.$$

If $U \ll U_c$, the Winkler foundation spring force b dominates the thin-shell spring force $c_l^2 d$, and (3.3) gives an $h_c = O(U^{8/3})$ power law,

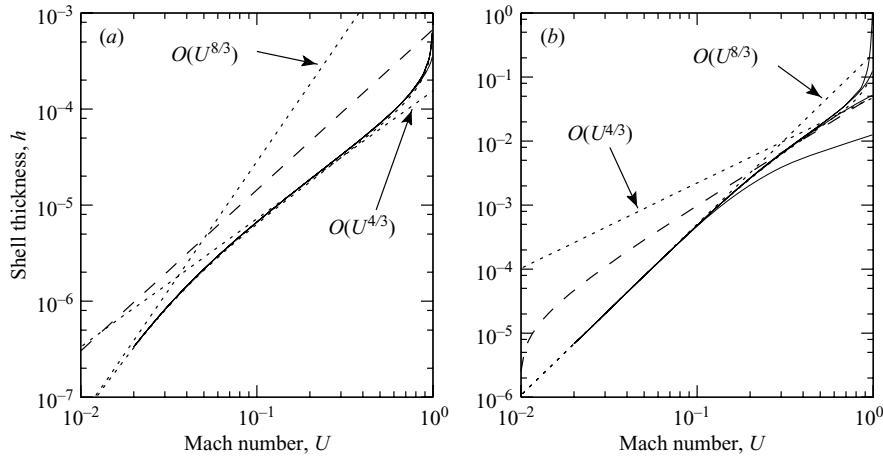$$h_c \simeq \frac{c_l^2 \rho_s}{b}\left(\frac{9U^4}{8c_l^4 \rho_s^2}\right)^{2/3}.$$

FIGURE 6. Comparison between asymptotic approximations and numerical results for h_c, for $b = 1$ and $m \in \{0, 1, 5, 24\}$, and (a) air within aluminium and (b) water within steel solid lines are numerical results, short dashed lines are (3.3) and the power laws derived from it, and long dashed lines are from Peake (1997).

Alternatively, if $U \gg U_c$ it is the thin-shell spring force that dominates, and we get an $h_c = O(U^{4/3})$ power law,

$$h_c \simeq \left(\frac{9U^4}{8c_l^4 \rho_s^2} \right)^{1/3}.$$

Note that if $b = 0$, corresponding to no Winkler foundation spring force, the $h_c = O(U^{4/3})$ power law is universally valid for $U \ll 1$.

Figure 6 compares these predictions against the numerically found values of h_c (as found for figure 5). As U approaches unity, the m^2/β^2 factor in (3.2) becomes significant, and the above asymptotics breaks down, provided $m \neq 0$. However, for small and moderate U, the asymptotics derived above show a very good agreement with the numerical results, and the $U^{8/3}$ and $U^{4/3}$ scaling laws are clearly demonstrated.

4. Scattering by a rigid-wall to thin-shell boundary transition

Consider the duct shown in figure 1, which for $x < 0$ has a rigid-wall boundary with boundary condition $\partial\phi/\partial r = 0$, while for $x > 0$ the boundary is a thin shell, as described by Flügge's equations. The thin-shell boundary is clamped to the rigid boundary at the intersection $x = 0$. All quantities are assumed proportional to $\exp\{i\omega t - im\theta\}$. A rigid-wall duct mode with pressure $p_{in}(x, r) = \exp\{-ik_{in}x\}J_m(\alpha_{in}r)/J_m(\alpha_{in})$ is inbound from upstream, where $\alpha_{in}^2 = (\omega - Uk_{in})^2 - k_{in}^2$ and $J'_m(\alpha_{in}) = 0$. Since this mode does not satisfy the boundary condition for $x > 0$, as it encounters the boundary transition it scatters into other duct modes, some of which are reflected back upstream. This situation is similar to the case considered by Rienstra (2007), although for a thin-shell boundary, and a similar method is used to solve for the scattered solution using the Wiener–Hopf technique, as described by Noble (1958).

4.1. *Solution in the fluid*

If $w(x)$ is the small unsteady radial deflection of the boundary, as shown in figure 1, then the governing equations and boundary condition on the fluid give

$$\frac{\mathrm{D}^2\phi}{\mathrm{D}t^2} - \nabla^2\phi = 0, \qquad \text{subject to} \qquad \frac{\partial\phi}{\partial r} = \frac{\mathrm{D}w}{\mathrm{D}t} \qquad \text{at } r = 1. \tag{4.1}$$

This boundary condition is the linearized 'no flow through the boundary' condition, valid for all x, and agrees with the Myers (1980) boundary condition since the steady flow is uniform. The total pressure is $p = -\mathrm{D}\phi/\mathrm{D}t = p_{\mathrm{in}} - \mathrm{D}\psi/\mathrm{D}t$, where ψ is the potential of the wave scattered by the impedance boundary change at $x = 0$ and p_{in} is the incident pressure.

In order to achieve a causal solution, and for the convergence of the integrals that follow, it turns out to be convenient to consider $\omega = \omega_r - \mathrm{i}\varepsilon$ with ω_r real, and ε positive and chosen such that $\mathrm{Im}(\omega(k)) > -\varepsilon$ for all real k. (In other words, we consider initially the scattering at a frequency ω which has a more negative imaginary part than any solution of the dispersion relation for ω in terms of k for real k.) Hence, for this ω, there are no modes with real k, and it is assumed that there exists some positive $\delta(\varepsilon)$ such that the strip $\mathscr{D}$ given by $|\mathrm{Im}(k)| < \delta$ is free of any rigid-wall or thin-shell modes. The Briggs–Bers criterion then dictates that, for this frequency, all modes that originate at $x = 0$ decay exponentially as $|x| \to \infty$, and from the definition of $\mathscr{D}$ it follows that they decay at least as fast as $\exp\{-\delta|x|\}$. It will also turn out to be useful to require δ to be small enough so that $\omega/(U \pm 1)$, k_l, and k_t all lie outside $\mathscr{D}$. Analytic continuity of the solution to $\varepsilon = 0$ will eventually be sought.

The Fourier transform of ψ is given by

$$\tilde{\psi}(k, r) = \int_{-\infty}^{\infty} \psi(x, r)\mathrm{e}^{\mathrm{i}kx} \, \mathrm{d}x,$$

which, because of the choice of ε, for k in $\mathscr{D}$ converges absolutely and is therefore analytic. The Fourier-transformed differential equation (4.1) is solved as before in terms of Bessel's functions, giving $\tilde{\psi}(k, r) = A(k)\mathrm{J}_m(\alpha(k)r)$, where $A(k)$ is an as yet undetermined function and $\alpha(k)^2 = (\omega - Uk)^2 - k^2$. The branch cuts for $\alpha(k)$ are taken parallel to the imaginary axis and away from the real axis, so that $\alpha(k)$ is analytic and $\mathrm{Im}(\alpha(k)) > 0$ in $\mathscr{D}$. These branch cuts will turn out to be unnecessary, as in §2. This will become apparent *a posteriori*, and is equivalent to the discrete modes forming a complete set.

For $x < 0$ the duct wall is rigid and therefore $w(x) \equiv 0$. The Fourier transform of $w(x)$ is therefore given by the positive-half-range transform

$$H^+(k) = \int_0^\infty w(x)\mathrm{e}^{\mathrm{i}kx} \, \mathrm{d}x,$$

which is an analytic function of k for $\mathrm{Im}(k) > -\delta$. For positive-half-range Fourier transforms, note that

$$\int_0^\infty f'(x)\mathrm{e}^{\mathrm{i}kx} \, \mathrm{d}x = -f(0) - \mathrm{i}k \int_0^\infty f(x)\mathrm{e}^{\mathrm{i}kx} \, \mathrm{d}x$$

assuming appropriate decay at infinity (which is ensured in all cases here by taking $k \in \mathscr{D}$). Hence, the boundary condition from (4.1) gives

$$\alpha(k)A(k)\mathrm{J}'_m(\alpha(k)) = \mathrm{i}(\omega - Uk)H^+(k), \tag{4.2}$$

yielding $A(k)$ in terms of the unknown function $H^+(k)$. Equation (4.1) is now satisfied, for any function $H^+(k)$, or equivalently for any boundary deflection $w(x)$. The physics of the boundary remain to be satisfied.

4.2. *Imposing the thin-shell boundary*

For a thin-shell boundary, the boundary deflection $w(x)$ is related to the fluid pressure $p(x, 1)$ at the boundary by Flügge's equations, the full-range Fourier transforms of which are given in (2.2). Here, we are interested in the positive-half-range Fourier transform of Flügge's equations, in order to derive $H^+(k)$. Since the thin shell is clamped at $x = 0$, so that $w(0) = w'(0) = u(0) = v(0) = 0$, the positive-half-range Fourier transforms of Flügge's equations give

$$\int_0^\infty p(x, 1)e^{ikx}\,dx = i\omega Z_1(k)H^+(k) + i\omega Z_0(k), \qquad (4.3)$$

where

$$i\omega Z_1(k) = c_l^2 d + b + i\omega R - d\omega^2 + B(k^2 + m^2)^2$$
$$- c_l^2 d \frac{A_1{}^2 a_{22} - 2A_1 A_2 a_{12} + A_2{}^2 a_{11}}{\left(\omega^2/c_l^2 - (k^2 + m^2)\right)\left(\omega^2/c_l^2 - \frac{1}{2}(1 - \nu)(k^2 + m^2)\right)}, \qquad (4.4)$$

$$i\omega Z_0(k) = ic_l^2 d \frac{A_1 C_1 a_{22} - (A_1 C_2 + A_2 C_1)a_{12} + A_2 C_2 a_{11}}{\left(\omega^2/c_l^2 - (k^2 + m^2)\right)\left(\omega^2/c_l^2 - \frac{1}{2}(1 - \nu)(k^2 + m^2)\right)} + iBC_3 k - BC_4, \quad (4.5)$$

$$C_1 = u'(0) - \frac{h^2}{12}w''(0), \qquad C_2 = \frac{1 - \nu}{2}v'(0),$$

$$C_3 = \left(1 - \frac{h^2}{12}\right)w''(0) - C_1, \quad C_4 = \left(1 - \frac{h^2}{12}\right)w'''(0) + 2imC_2.$$

The equality $u''(0) = w'''(0)h^2/12 + imv'(0)(1 + \nu)/2$, implied by the axial component of Flügge's equations, has been used to write C_4 in the given form. These constants bear a great similarity to the forces and moments exerted on the hard-wall section by the thin shell at the clamp at $x = 0$.

Since the positive-half-range transform of $p_{\text{in}}(x, 1)$ is $i/(k - k_{\text{in}})$, the positive-half-range transform of $p(x, 1)$ may be manipulated to give

$$\int_0^\infty p(x, 1)e^{ikx}\,dx = \frac{i}{k - k_{\text{in}}} - i(\omega - Uk)A(k)J_m(\alpha(k)) - P^-(k), \qquad (4.6)$$

where $P^-(k)$ is the negative-half-range Fourier transform of the scattered pressure at the boundary,

$$P^-(k) = \int_{-\infty}^0 -\frac{D\psi}{Dt}(x, 1)e^{ikx}\,dx,$$

and is analytic for $\text{Im}(k) < \delta$. Equating (4.6) and (4.3) gives

$$P^-(k) - i/(k - k_{\text{in}}) + i\omega Z_0(k) = H^+(k)K(k), \qquad (4.7)$$

where

$$K(k) = \frac{(\omega - Uk)^2 J_m(\alpha(k))}{\alpha(k)J'_m(\alpha(k))} - i\omega Z_1(k) \qquad (4.8)$$

is the Wiener–Hopf kernel. Equations (4.7) and (4.8) form the Wiener–Hopf problem.

4.3. *Solving the Wiener–Hopf problem*

In order to solve this Wiener–Hopf problem, the poles of the Wiener–Hopf kernel $K(k)$ must be investigated. $K(k)$ has poles which are zeros of $J'_m(\alpha(k))$, zeros of $\alpha(k)$, or poles of $i\omega Z_1$. Zeros of $J'_m(\alpha(k))$ correspond to rigid-wall duct modes, while the poles of $i\omega Z_1$ are due to the determinant of (2.2b) being zero, and occur at $\pm k_l$ and $\pm k_t$. The zeros of $K(k)$ are given by the zeros of $\chi(k)$, where

$$\chi(k) = (\omega - Uk)^2 J_m(\alpha(k)) - i\omega Z_1(k)\alpha(k)J'_m(\alpha(k)), \tag{4.9}$$

and hence correspond to duct modes for a duct boundary with impedance Z_1 (cf. (2.1)). Hence, by definition of ε, the strip $\mathscr{D}$ defined by $|\text{Im}(k)| < \delta$ contains no poles or zeros of $K(k)$. As described in the Appendix, this kernel may therefore be factorized into $K(k) = K^+(k)/K^-(k)$, where $K^+(k)$ is analytic for $\text{Im}(k) > -\delta$, and $K^-(k)$ is analytic for $\text{Im}(k) < \delta$. Similarly, $i\omega Z_0(k)K^-(k)$ may be split into $F^-(k) + F^+(k)$. Substituting these factorizations into (4.7) yields

$$P^-(k)K^-(k) - \frac{i(K^-(k) - K^-(k_{\text{in}}))}{k - k_{\text{in}}} + F^-(k) = H^+(k)K^+(k) + \frac{iK^-(k_{\text{in}})}{k - k_{\text{in}}} - F^+(k). \tag{4.10}$$

The left-hand side is analytic for $\text{Im}(k) < \delta$, while the right-hand side is analytic for $\text{Im}(k) > -\delta$. Hence, the above defines an entire function $E(k)$.

From the Appendix, the following asymptotic behaviour is found as $|k| \to \infty$ in the regions of analyticity:

$$K^-(k) = O(k^{-2}), \quad F^-(k) = O(k^{-1}), \quad K^+(k) = O(k^2), \quad F^+(k) = O(k^{-1}).$$

Assuming the fluid pressure at the duct boundary at $x = 0$ to be finite, $P^-(k) = O(k^{-1})$, while the clamped boundary conditions $w(0) = w'(0) = 0$ imply $H^+(k) = O(k^{-3})$. Hence, both the left- and right-hand sides of (4.10) are $O(k^{-1})$ as $|k| \to \infty$, and so by Liouville's theorem the entire function $E(k) \equiv 0$.

Setting the right-hand side of (4.10) to zero gives an equation for $H^+(k)$, from which (4.2) gives the scattering wave spectrum $A(k)$. Hence, the total pressure field is found to be

$$p(x, r) = p_{\text{in}}(x, r) + \frac{1}{2\pi i} \int_{-\infty}^{\infty} \frac{(\omega - Uk)^2 J_m(\alpha(k)r)}{\alpha(k)J'_m(\alpha(k))K^+(k)} \left[\frac{K^-(k_{\text{in}})}{k - k_{\text{in}}} + \frac{iR_l}{k - k_l} + \frac{iR_t}{k - k_t} \right] e^{-ikx} \, dk, \tag{4.11}$$

where

$$\left. \begin{array}{l} R_l = \frac{ic_l^2 dK^-(k_l)}{2k_l\omega^2/c_l^2} \left(k_l^2 \left(\nu + \frac{h^2\omega^2}{12c_l^2} \right) + m^2 \right) (k_l C_1 + m C_2), \\[2mm] R_t = \frac{ic_l^2 dK^-(k_t)}{2\omega^2/c_l^2} m \left(1 - \nu + \frac{h^2\omega^2}{12c_l^2} \right) (k_t C_2 - m C_1). \end{array} \right\} \tag{4.12}$$

are from $F^+(k)$ (see equation (A 2) in the Appendix). Since the integrand is $O(k^{-2})$ as $|k| \to \infty$, for $x < 0$ the integration contour may be closed in the upper half-plane and Jordan's lemma applied. The contour must be deformed around the branch cut of α in the upper half-plane. However, since $J_m(\alpha r)/(\alpha J'_m(\alpha))$ is a meromorphic function of α^2, the integrand is identical on either side of the branch cut and the contribution from integrating around the branch cut vanishes. The singularity at $\alpha = 0$ corresponds to a removable singularity for $m \neq 0$, while for $m = 0$ it is included in the following analysis provided it is taken that $m^2/\alpha^2 = 0$. The integral is therefore $2\pi i$ times the sum of the residues of the integrand in the upper half-plane. These poles are given by $J'_m(\alpha(k)) = 0$ and correspond to rigid-wall duct modes. Denoting the jth positive

root of $J'_m(\alpha) = 0$ by $\alpha_{jm} = \alpha(k_{jm})$ with $\mathrm{Im}(k_{jm}) > 0$, for $x < 0$ the total pressure is given by

$$p(x, r) = \frac{J_m(\alpha_{\mathrm{in}} r)}{J_m(\alpha_{\mathrm{in}})} \exp\{-\mathrm{i}k_{\mathrm{in}} x\} + \sum_{j=1}^{\infty} R_{jm} \frac{J_m(\alpha_{jm} r)}{J_m(\alpha_{jm})} \exp\{-\mathrm{i}k_{jm} x\}, \qquad (4.13)$$

where

$$R_{jm} = \frac{(\omega - Uk_{jm})^2}{(U\omega + \beta^2 k_{jm})(1 - m^2/\alpha_{jm}^2) K^+(k_{jm})} \left[\frac{K^-(k_{\mathrm{in}})}{k_{jm} - k_{\mathrm{in}}} + \frac{\mathrm{i}R_l}{k_{jm} - k_l} + \frac{\mathrm{i}R_t}{k_{jm} - k_t} \right].$$

Similarly, for $x > 0$ the integration contour in (4.11) may be closed in the lower half-plane and Jordan's lemma applied. Writing $\alpha J'_m(\alpha) K^+(k)$ as $K^-(k)\chi(k)$, where $\chi(k)$ is given in (4.9), the poles of the integrand of (4.11) are given by zeros of $\chi(k)$, and therefore correspond to duct modes for a duct boundary with impedance Z_1. The pole at k_{in} exactly cancels the incoming pressure p_{in}. The two poles at k_l and k_t correspond to zeros of the determinant (2.2b), so are also poles of $\chi(k)$; the integrand therefore has removable singularities at these points. Denoting the jth zero of $\chi(k)$ by τ_{jm} with $\mathrm{Im}(\tau_{jm}) < 0$, the pressure for $x > 0$ is given by

$$p(x, r) = \sum_{j=1}^{\infty} T_{jm} \frac{J_m(\alpha(\tau_{jm}) r)}{J_m(\alpha(\tau_{jm}))} \exp\{-\mathrm{i}\tau_{jm} x\}, \qquad (4.14)$$

where

$$T_{jm} = -\frac{(\omega - U\tau_{jm})^2 J_m(\alpha(\tau_{jm}))}{K^-(\tau_{jm})\chi'(\tau_{jm})} \left[\frac{K^-(k_{\mathrm{in}})}{\tau_{jm} - k_{\mathrm{in}}} + \frac{\mathrm{i}R_l}{\tau_{jm} - k_l} + \frac{\mathrm{i}R_t}{\tau_{jm} - k_t} \right].$$

The solution within the fluid has now been derived as a sum of duct modes, with reflection coefficients R_{jm} and transmission coefficients T_{jm}, in terms of the constants C_1 and C_2.

4.4. *Determining the constants C_1 to C_4*

By examining (4.11), the dependence of the solution on the constants C_1 to C_4 occurs only through R_l and R_t, which themselves depend only on C_1 and C_2 and are independent of C_3 and C_4. In fact C_3 and C_4 may be calculated (in terms of C_1 and C_2) from our solution for H^+, since by integrating by parts

$$H^+(k) = -\mathrm{i}w''(0)/k^3 + w'''(0)/k^4 + O(k^{-5}) \quad \text{as } k \to \infty, \qquad (4.15)$$

giving $w''(0)$ and $w'''(0)$, and hence C_3 and C_4. This is possible because, in determining H^+, we required the pressure to be bounded at $x = 0$, implying $P^-(k) = O(k^{-1})$ as $|k| \to \infty$. In general, however, setting the left-hand side of (4.10) to zero gives $P^-(k) = O(k)$. Satisfying the finite pressure assumption therefore requires the constants C_3 and C_4 to be chosen such that

$$-\frac{\mathrm{i}K^-(k_{\mathrm{in}})}{k - k_{\mathrm{in}}} + F^+(k) = \mathrm{i}\omega Z_0 K^-(k) + O(k^{-3}),$$

and this can be shown to give the same condition as (4.15). This may be interpreted as the shell bending at $x = 0$ in the only way that does not necessitate an infinite pressure in the fluid at the boundary. As C_3 and C_4 do not appear in the solution (4.11), it is never necessary to solve the above equations to calculate C_3 and C_4, and we may now forget about C_3 and C_4 completely.

We now turn our attention to the constants C_1 and C_2, which we determine by imposing causality. The inversion contour in (4.11) is chosen along the real-k-axis within the strip $\mathscr{D}$. By definition of ε, the Briggs–Bers criterion shows that this gives the causal solution to a disturbance in the fluid originating at $x = 0$. However, the solid waves in the boundary with axial wavenumbers $\pm k_l$ and $\pm k_t$ are decoupled from w and produce no disturbance in the fluid for $x > 0$. It is therefore necessary to impose a further condition that no solid waves are inbound in the boundary from $x = +\infty$. The positive-half-range Fourier transforms of the axial and azimuthal boundary displacements $u(x)$ and $v(x)$ for $x > 0$ are denoted $U^+(k)$ and $V^+(k)$, and are given by the half-range version of (2.2*b*) as

$$
\begin{pmatrix} U^+ \\ V^+ \end{pmatrix} = \frac{1}{a_{11}a_{22} - a_{12}{}^2} \begin{pmatrix} a_{22} & -a_{12} \\ -a_{12} & a_{11} \end{pmatrix} \begin{pmatrix} -\mathrm{i}A_1 H^+ - C_1 \\ -\mathrm{i}A_2 H^+ - C_2 \end{pmatrix}. \tag{4.16}
$$

This shows that $U^+(k)$ and $V^+(k)$ are $O(k^{-2})$ as $|k| \to \infty$. Taking the inversion contours for $u(x)$ and $v(x)$ above all poles of U^+ and V^+, Jordan's lemma may be applied to give $u \equiv v \equiv 0$ for $x < 0$, while for $x > 0$, u and v are given as a sum of residues. In general, the poles of U^+ and V^+ are those of H^+. The zeros of the determinant $a_{11}a_{22} - a_{12}{}^2$, which occur when $k = \pm k_l$ or $k = \pm k_t$, lead to four additional poles of U^+ and V^+ which correspond to two inbound and two outbound solid boundary waves. In order that there be no incoming waves, it is required that the poles of U^+ and V^+ at both $-k_l$ and $-k_t$ have zero residue (recall that k_l and k_t were chosen so as to represent downstream-propagating waves). While this would appear to be four conditions, the singularity of the matrix at these points reduces this requirement to two conditions,

$$
k_l(\mathrm{i}A_1(-k_l)H^+(-k_l) + C_1) - m(\mathrm{i}A_2(-k_l)H^+(-k_l) + C_2) = 0,
$$
$$
m(\mathrm{i}A_1(-k_t)H^+(-k_t) + C_1) + k_t(\mathrm{i}A_2(-k_t)H^+(-k_t) + C_2) = 0.
$$

Since $H^+(k)$ is a linear function of C_1 and C_2, so too are the above two equations. Satisfying them specifies the constants C_1 and C_2 (which in turn specifies $u'(0)$ and $v'(0)$), and ensures that the only permissible solid boundary waves are those that propagate outward from $x = 0$.

It is interesting to note that outward-propagating solid boundary waves, corresponding to the other two zeros of the determinant in (4.16) at $k = k_l$ and $k = k_t$, both have zero residue for any choice of C_1 and C_2. This may be seen by evaluating H^+ at k_l and k_t to give

$$
H^+(k_l) = \mathrm{i}\frac{k_l C_1 + mC_2}{k_l A_1(k_l) + m A_2(k_l)} \qquad \text{and} \qquad H^+(k_t) = \mathrm{i}\frac{mC_1 - k_t C_2}{m A_1(k_t) - k_t A_2(k_t)},
$$

and substituting this into (4.16). The poles at k_l and k_t therefore correspond to removable singularities, and once C_1 and C_2 have been chosen as above so that the poles at $-k_l$ and $-k_t$ also correspond to removable singularities, the only poles of U^+ and V^+ are those of H^+. The wave scattering is therefore seen to excite none of the solid waves in the thin shell, although it can, and in general will, excite the quasi-solid surfaces modes in the fluid.

The values of all four constants C_1 to C_4 have now been specified, giving a unique solution, with the only assumptions being bounded pressure and causality. Since the thin shell was assumed clamped at $x = 0$, $w(0) = w'(0) = 0$, and hence the deflection of the surface streamline is $O(x^2)$ as $x \to 0$.
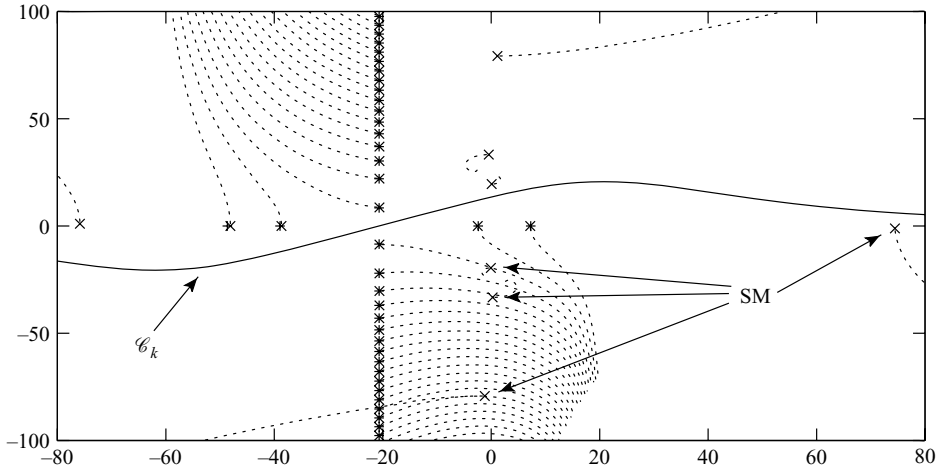
FIGURE 7. Rigid-wall ($+$) and thin-shell ($\times$) modes in the k-plane. Dashed lines show the Briggs–Bers trajectories. Surfaces modes for $x > 0$ are labelled SM. Parameters are as for figure 2.

4.5. *Analytic continuation to real frequencies*

So far, $\mathrm{Im}(\omega) = -\varepsilon$ has been taken, with the results for real ω to be inferred by analytic continuation in the limit $\varepsilon \to 0$. In this limit the rigid-wall modes approach the real-k-axis, and the factorizing contour and the strip $\mathscr{D}$ must therefore be deformed around such modes to maintain analyticity. This is exactly the same situation as for the Briggs–Bers criterion; in other words, in choosing the position of the contours and the strip $\mathscr{D}$, it is necessary to consider the stability of the modes. It is also necessary for k_l and k_t to lie below and $-k_l$ and $-k_t$ to lie above $\mathscr{D}$, since $H^+(-k_l)$, $H^+(-k_t)$, $K^-(k_l)$ and $K^-(k_t)$ appear in the solution, and H^+ is only defined above the factorizing contour, while K^- is only defined below it. From a Briggs–Bers point of view, this may be seen as requiring k_l and k_t to be right-propagating and $-k_l$ and $-k_t$ to be left-propagating.

5. Numerical results

Figure 7 shows the numerically calculated rigid-wall and thin-shell poles in the k-plane for an air-filled aluminium duct (see table 1) of 1 m radius and 1 mm shell thickness, with ω and m as suggested by McAlpine & Wright (2006) as being representative of rotor-alone fan noise in aeroengine intakes. For details of the numerical procedure, see the Appendix §A.2. The majority of thin-shell modes are almost identical to their rigid-wall counterparts, apart from the eight surface modes. The Briggs–Bers stability analysis has been superimposed on figure 7, showing the motion of the thin-shell modes as ε is varied, and consequently the stability of these modes may be verified; it was shown in §3 that the Briggs–Bers criterion is valid in this case, and that no absolute or convective instabilities are present. The factorizing contour and the inversion contour coincide and are labelled $\mathscr{C}_k$, which has been chosen both to give the correct stability and also with regard to k_l and k_t. The equation of this curve (following Rienstra 2007) is

$$k = \frac{\omega}{1 - U^2} \left(\xi - U + \mathrm{i} Y \frac{4(\xi/q)}{3 + (\xi/q)^4} \right), \quad \xi \in \mathbb{R}, \tag{5.1}$$

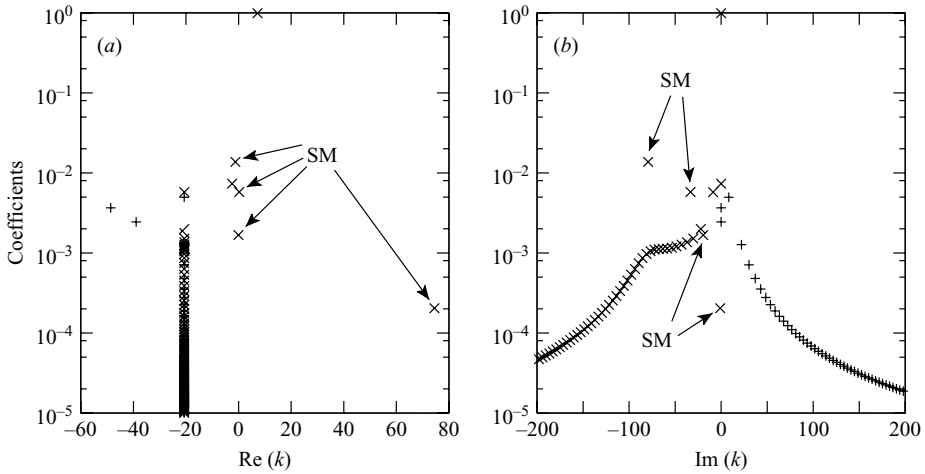with in this case $Y = 0.5$ and $q = 1.0$.

FIGURE 8. Scattering coefficients $|R_{jm}|$ (+) and $|T_{jm}|$ (×) for an inbound first-radial-order mode. Parameters are as for figure 7.
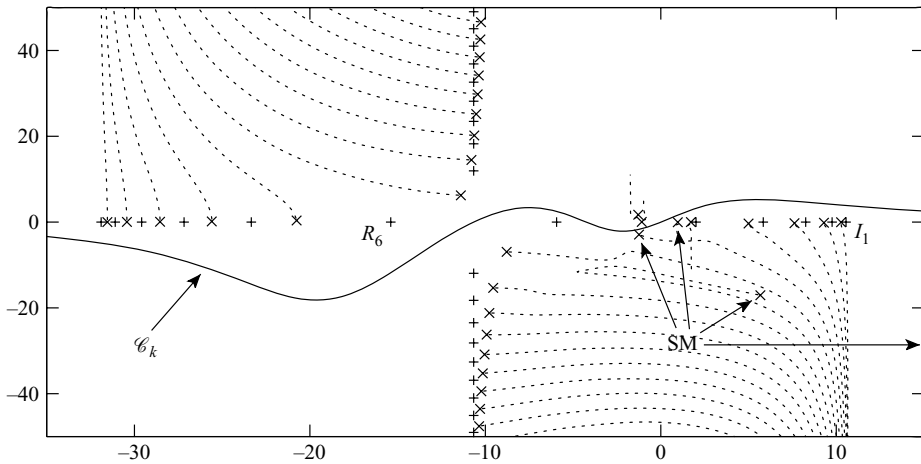

FIGURE 9. Rigid-wall (+) and thin-shell (×) modes in the k-plane. Dashed lines are the Briggs–Bers trajectories for the thin-shell modes. One of the surface modes (labelled SM) is not shown owing to the scale used. The fluid is air and the boundary is aluminium, with $U = 0.5$, $R = 0.5$, $b = 0$, $m = 1$, $\omega = 16$, and $h = 10^{-4}$.

Figure 8 shows the numerically evaluated scattering response to an inbound first-radial-order mode for the parameters used in figure 7. It shows the response to the inbound mode is dominated by the first-radial-order thin-shell mode, with little scattering or reflection taking place.

As a second example, for what follows the parameters used are $U = 0.5$, $R = 0.5$, $b = 0$, $m = 1$, and $\omega = 16$, for a 1 m radius aluminium duct with boundary thickness 0.1 mm, for which it may be checked (or inferred from figure 5) that no instabilities are present. The rigid-wall and thin-shell modes in the k-plane are shown in figure 9, with the Briggs–Bers trajectories showing the $\mathscr{C}_k$ contour to have been chosen to give the correct stability. The simple $\mathscr{C}_k$ contour in (5.1) does not provide enough flexibility
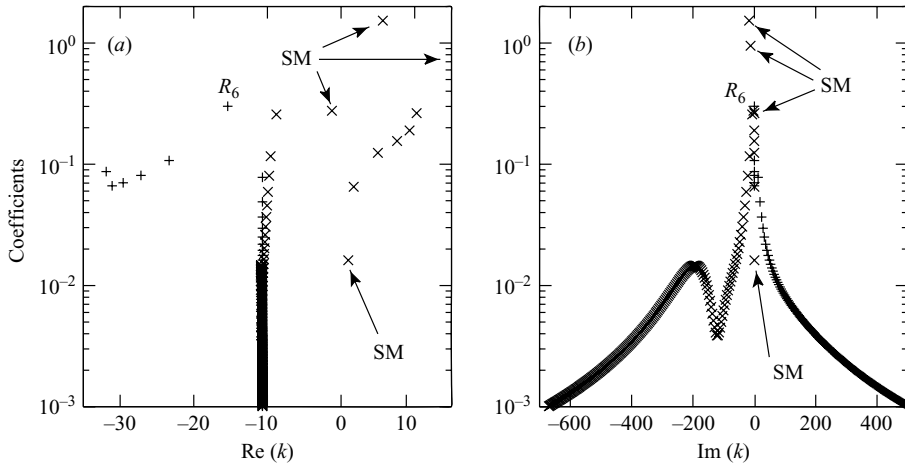
FIGURE 10. Scattering coefficients $|R_{jm}|$ (+) and $|T_{jm}|$ (×) due to an incoming first-radial-order rigid-wall mode I_1. Parameters are as for figure 9.
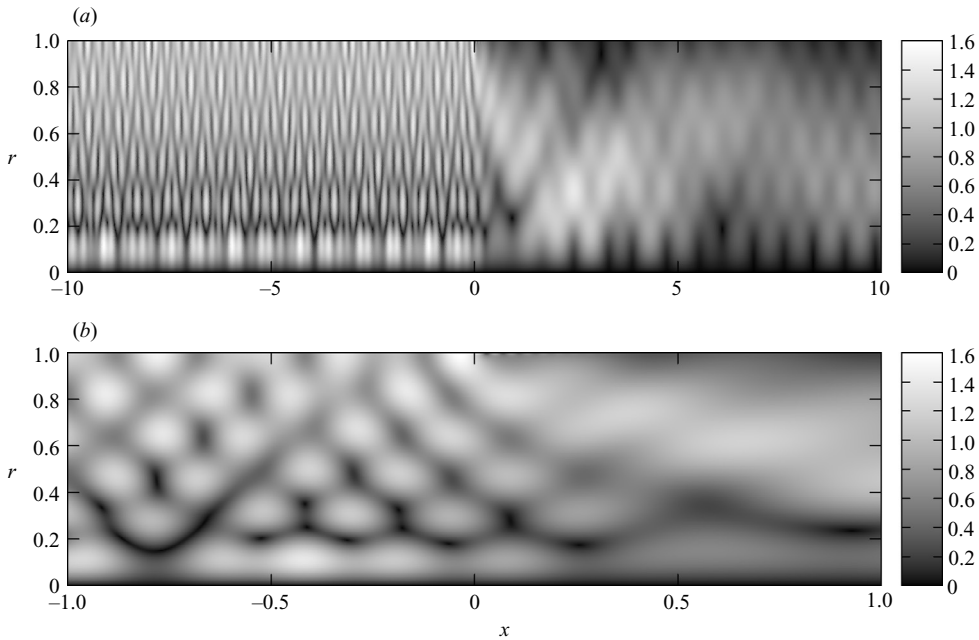

FIGURE 11. Amplitude of pressure oscillations $|p(r, x)|$ due to an inbound I_1 mode. (b) A more detailed plot of (a). Parameters are as for figure 9. An animation of this figure is given in movie 1, available with the online version of the paper.

to do this, and the more general contour given by

$$k = \frac{\omega}{1 - U^2} \left[\xi - U + \mathrm{i} Y \frac{4(\xi/q)}{3 + (\xi/q)^4} \left(1 - \frac{1 + g}{1 + g(\xi/f + 1 - U/f)^2} \right) \right], \quad \xi \in \mathbb{R} \quad (5.2)$$

was used, with $Y = 1.0$, $q = 0.4$, $f = 0.1$, and $g = 0.1$.

Figure 10 shows the scattering response for the incoming first-radial-order mode labelled I_1 in figure 9. The surface modes play a major role near $x = 0$ in order to

match the rigid-wall and thin-shell solutions smoothly, although their fast decay means they have a negligible effect away from $x = 0$. For large positive x the dominant mode is the first-radial-order thin-shell mode. However, note also the comparably large coefficient for the sixth-radial-order reflected (left-propagating) mode labelled R_6, showing that both transmission and reflection are important in this situation. Figure 11 shows the amplitude of pressure oscillations, obtained from summing the above coefficients. In $x < 0$, the sum of two modes is prominently seen: the inbound first-radial-order I_1 mode (maximum amplitude at $r = 1$ and zero amplitude at $r = 0$), and the sixth-radial-order R_6 reflected mode (visible as six horizontal bands). This may be seen more clearly in movie 1, available as a supplement to the online version of the paper, which is an animation of figure 11. Figure 11(b) shows a more detailed view around the boundary transition at $x = 0$ where the surface modes are important, and demonstrates the continuity between $x < 0$ and $x > 0$ which is less apparent in figure 11(a). Since solutions for $x < 0$ and $x > 0$ are calculated by summing two different series, (4.13) and (4.14), this continuity provides a good check on the numerical results. The surface streamline was also calculated for this example (by numerically summing the poles in the inverse transform of H^+) and showed the predicted $O(x^2)$ behaviour at $x = 0$.

6. Conclusion

The mass–spring–damper boundary model is inappropriate for stability analysis, since $\text{Im}(\omega(k))$ is not bounded below for real k, and hence the Briggs–Bers criterion is inapplicable. The same problem occurs with a Helmholtz resonator or enhanced Helmholtz resonator boundary model (as described by Rienstra 2006). In fact, problems for which $\text{Im}(\omega(k))$ is not bounded below for real k are ill-posed, since they do not satisfy the conditions of the Hille–Yosida theorem (Rudin 1991), and so do not generate a continuous semigroup; in other words, there are initial conditions for which the solution at $t = 0$ does not match with the solution at $t = \varepsilon$ in the limit $\varepsilon \to 0$. There may not even be a sensible answer to the question of spatial stability given a time-harmonic forcing for such problems, although they are certainly temporally unstable for some initial conditions. The ill-posedness is also prevalent in computer simulations. It is known (e.g. Tam & Auriault 1996) that time-domain numerical calculations using the mass-spring-damper boundary are unstable, with the instability wavelength comparable with the grid scale, and therefore the instability changes as the grid is refined. Consequently, such instabilities are routinely filtered out using a low-pass filter (Tam & Auriault 1996; Chevaugeon, Remacle & Gallez 2006; Tam & Ju 2006; Richter & Thiele 2007). However, we can now see that such an instability is caused by the numerics attempting to realize the underlying arbitrarily quickly growing absolute instability at arbitrarily small wavelengths.

A regularization of such boundary conditions that is well-posed is obviously needed, particulary in the light of the interpretation by Brandes & Ronneberger (1995) that they observe instablities in their experimental results (although the instability is restricted to a short leading section of the lined duct and decays after this, so is very different in nature to the instability suggested by Rienstra 2003). In this paper, the problem is regularized by considering the boundary as a thin shell, as described by Flügge's equations. The influence of bending stiffness bounds $\text{Im}(\omega(k))$ below for real k, enabling the Briggs–Bers criterion to be applied. The mass–spring–damper model is obtained in the limit $h \to 0$. The ill-posedness mentioned above manifests itself as an absolute instability of frequency ω_p with $\text{Im}(\omega_p) \to -\infty$ as $h \to 0$. Consequently,

the solution to a time-harmonic forcing turned on at $t = 0$ grows arbitrarily fast in time as $h \to 0$. This also ties in with the surface mode behaviour, since there are two real surface modes whose wavenumbers tend to infinity as $h \to 0$, and that are not included in the mass–spring–damper model.

The mass–spring–damper model was used by Rienstra (2003) as a model of an acoustic lining in an aeroengine. Of course, the thin-shell boundary is a model of a different physical system, and we do not suggest that real acoustic liners might be modelled as thin shells. However, what we have shown is that modifying the boundary condition for large k with the inclusion of bending stiffness, while replicating mass–spring–damper-like behaviour for small and moderate k (see figure 3), enables a rigorous stability analysis which leads to different conclusions about stability from those reached for the mass–spring–damper system. In addition, the scattering behaviour for a thin-shell boundary ($O(x^2)$ wall-streamline continuity) is neither the behaviour of the mass–spring–damper boundary with an instability ($O(x^{3/2})$), nor of the mass–spring–damper boundary without an instability ($O(x^{1/2})$), demonstrating that regularizing the problem is important for more than simply determining stability. We suggest that, in order to perform a stability or scattering analysis on a model of an acoustic lining, the model needs to be modified in some way to include a k dependence in the impedance Z, such that $\mathrm{Im}(\omega(k))$ is bounded below for real k (as was also suggested by Brandes & Ronneberger 1995). For example, if ℓ is the length scale of some small-scale feature of the acoustic lining, such as the length scale of the perforations of the facing sheet or the thickness of the boundary layer, then different behaviour may well result for $k\ell \gg 1$.

From a fluid-loaded structures perspective, the incompressible stability analysis of Peake (1997) has been extended to account for compressible effects; it has been found that, for the parameters considered, the system exhibits either stable or absolutely unstable behaviour, but not solely convective instability. The boundary between absolute instability and stable behaviour is best summarized by figure 5 (the equivalent of figure 2 in Peake 1997, although with a different non-dimensionalization). The inclusion of compressibility has been shown to have a marked effect on the absolute instability boundary, and the small-U incompressible predictions (Peake 1997, equation ((3.3)), which were very accurate in the incompressible case, are less accurate in the compressible case. In the small-U limit, we have found the critical shell thickness for instability to behave as $O(U^{8/3})$ or $O(U^{4/3})$, depending on whether the Winkler foundation spring force is important or not, while in the incompressible case the scaling is $O(U^{5/3})$. In deriving our asymptotic predictions, we have assumed that the $m^2/(1 - U^2)$ terms could be neglected (which breaks down if both $U \approx 1$ and $m \neq 0$) and that $\omega_p = 0$ on the absolute instability boundary. The latter assumption has been true in all examples we considered, although no mathematical argument has been given as to why this should be the case.

There remains a large amount of parameter space for which we have not investigated stability. For example, interesting behaviour might be found for $c_l < 1$ (a highly compressible boundary), $\rho_s < 1$ (a flimsy boundary), or $U > 1$ (supersonic mean flow), all of which have been neglected in the present study.

Appendix. Details of the Wiener–Hopf scattering problem

A.1. *Factorizing the Wiener–Hopf kernel*

It is required to factorize $K(k)$, defined in (4.8), such that $K(k) = K^+(k)/K^-(k)$, where $K^+(k)$ is analytic and non-zero for $\mathrm{Im}(k) > -\delta$ and $K^-(k)$ is analytic and non-zero for $\mathrm{Im}(k) < \delta$. The method used here is as described by Noble (1958), and is very similar to the method used by Rienstra (2007). It follows from (4.4) that $K(k) = -B(1 - h^2/12)k^4 + O(k^2)$ as $|k| \to \infty$. Hence,

$$L(k) \equiv -\frac{K(k)}{B(1 - h^2/12)(k^2 + X^2)^2} = 1 + O(k^{-2}),$$

where $X > \delta$ is an arbitrary real positive constant. Since both $K(k)$ and $(k^2 + X^2)^2$ are analytic and non-zero in the strip $\mathscr{D}$, so too is $L(k)$, and hence $\log L$ may be defined so as to be analytic in $\mathscr{D}$. Using Cauchy's integral representation,

$$2\pi\mathrm{i}\log(L(k)) = \int_{-Y-\mathrm{i}\delta}^{Y-\mathrm{i}\delta} + \int_{Y-\mathrm{i}\delta}^{Y+\mathrm{i}\delta} + \int_{Y+\mathrm{i}\delta}^{-Y+\mathrm{i}\delta} + \int_{-Y+\mathrm{i}\delta}^{-Y-\mathrm{i}\delta} \frac{\log(L(\xi))}{\xi - k}\,\mathrm{d}\xi,$$

where the integration contours are straight lines between the endpoints, and k lies inside this closed contour. Since $\log(L(\xi))/(\xi - k) = O(\xi^{-3})$, the end integrals tend to zero as $Y \to \infty$ and the other two integrals converge, so that

$$\log(L(k)) = \frac{1}{2\pi\mathrm{i}} \int_{-\infty-\mathrm{i}\delta}^{\infty-\mathrm{i}\delta} \frac{\log(L(\xi))}{\xi - k}\,\mathrm{d}\xi - \frac{1}{2\pi\mathrm{i}} \int_{-\infty+\mathrm{i}\delta}^{\infty+\mathrm{i}\delta} \frac{\log(L(\xi))}{\xi - k}\,\mathrm{d}\xi. \tag{A 1}$$

The first integral is analytic for $\mathrm{Im}(k) > -\delta$, and similarly the second integral is analytic for $\mathrm{Im}(k) < \delta$. Calling the first integral $\log(L^+(k))$ and the second integral $\log(L^-(k))$ gives the decomposition $L(k) = L^+(k)/L^-(k)$. Hence

$$K^+(k) = \mathrm{i}(B(1 - h^2/12))^{1/2}(k + \mathrm{i}X)^2 L^+(k),$$
$$K^-(k) = -\mathrm{i}(B(1 - h^2/12))^{-1/2}(k - \mathrm{i}X)^{-2} L^-(k),$$

gives the required decomposition $K(k) = K^+(k)/K^-(k)$. Noble (1958, p. 15, theorem C) states that L^+ and L^- found using this method remain bounded as $|k| \to \infty$ provided $\log L = O(k^{-q})$ as $|k| \to \infty$ for $q > 0$. Here, $\log L = O(k^{-2})$, and so $L^+(k)$ and $L^-(k)$ are both $O(1)$ as $|k| \to \infty$; hence, $K^+(k) = O(k^2)$ and $K^-(k) = O(k^{-2})$.

Requiring $K^+/K^- = K$ with K^+ and K^- analytic and non-zero in their respective half-planes determines K^+ and K^- up to multiplication by an arbitrary analytic non-zero function. Since the asymptotic behaviour of these specific K^+ and K^- is known, they are in fact specified up to multiplication by an arbitrary constant. This is the degree of freedom provided by the arbitrary constant X above. However, such a constant has no effect on the final solution, as can be seen from (4.11).

The decomposition of $\mathrm{i}\omega Z_0(k)K^-(k)$ into $F^+(k) + F^-(k)$ is more straightforward. The only poles of $\mathrm{i}\omega Z_0(k)K^-(k)$ in the lower half-plane are the simple poles of $\mathrm{i}\omega Z_0$ at k_l and k_t. Hence, $F^-(k) = \mathrm{i}\omega Z_0(k)K^-(k) - F^+(k)$, where

$$F^+(k) = \frac{R_l}{k - k_l} + \frac{R_t}{k - k_t}, \tag{A 2}$$

and R_l and R_t are the residues of $\mathrm{i}\omega Z_0(k)K^-(k)$ at k_l and k_t, as given in (4.12). The large-k behaviour of F^+ and F^- is easily derived from (4.5), (A 2), and the asymptotic behaviour of $K^-(k)$, giving $F^+(k) = O(k^{-1})$ and $F^-(k) = O(k^{-1})$ as $|k| \to \infty$.

A.2. *Numerical evaluation*

Our first task is to compute the locations of the poles k_{jm} and τ_{jm}, as defined in §4.3. The values of k_{jm} were obtained using a Newton–Raphson iteration to find the (real) roots α_{jm} of $J'_m(\alpha) = 0$, using asymptotics from Abramowitz & Stegun (1964, p. 371) as starting points for the iteration. The values of τ_{jm} were obtained using a Newton–Raphson iteration to find the roots of $\chi(k) = 0$, using k_{jm} and the surface mode asymptotics of §2.2 as starting points. In addition, a grid of starting points was used to discover any other thin-shell modes not close to these starting points.

The factorization of $K(k)$ into $K^+(k)/K^-(k)$ was done by numerically integrating (A 1) along a contour $k(\xi)$ with $\xi \in \mathbb{R}$ (see equations (5.1) and (5.2)), using a change of variables $\xi = s/(1 - s^2)$ to get a finite integration range $s \in (-1, 1)$. Care must be taken to ensure that the numerically calculated $\log(L(\xi))$ remains analytic along the contour, and does not jump by a multiple of $2\pi i$ at any point. The coefficients R_{jm} and T_{jm} were then calculated, and finally the modes were summed to give the total pressure. The summations were truncated once the magnitude of the coefficients became sufficiently small; for example, figure 8(*b*) shows how the reflection and transmission coefficients decay as $|\mathrm{Im}(k)|$ increases.

REFERENCES

ABRAMOWITZ, M. & STEGUN, I. A. 1964 *Handbook of Mathematical Functions*, 9th edn. Dover.

BERS, A. 1983 Space–time evolution of plasma instabilities — absolute and convective. In *Basic Plasma Physics* (ed. A. A. Galeev & R. N. Sudan), *Handbook of Plasma Physics*, vol. 1, pp. 451–517. North-Holland.

BRAMBLEY, E. J. & PEAKE, N. 2006 Classification of aeroacoustically relevant surface modes in cylindrical lined ducts. *Wave Motion* **43**, 301–310.

BRANDES, M. & RONNEBERGER, D. 1995 Sound amplification in flow ducts lined with a periodic sequence of resonators. *AIAA Paper* 95–126.

BRIGGS, R. J. 1964 *Electron-Stream Interaction with Plasmas*, chap. 2. MIT Press.

CHEVAUGEON, N., REMACLE, J.-F. & GALLEZ, X. 2006 Discontinuous Galerkin implementation of the extended Helmholtz resonator model in time domain. *AIAA Paper* 2006-2569.

CRIGHTON, D. G. & LEPPINGTON, F. G. 1974 Radiation properties of the semi-infinite vortex sheet: the initial-value problem. *J. Fluid Mech.* **64**, 393–414.

CRIGHTON, D. G. & OSWELL, J. E. 1991 Fluid loading with mean flow. I. Response of an elastic plate to localized excitation. *Phil. Trans. R. Soc. Lond.* A **335**, 557–592.

GOLDSTEIN, M. E. 1978 Unsteady vortical and entropic distortions of potential flows round arbitrary obstacles. *J. Fluid Mech.* **89**, 433–468.

JONES, D. S. 1977 The scattering of sound by a simple shear layer. *Phil. Trans. R. Soc. Lond.* A **284**, 287–328.

JONES, D. S. & MORGAN, J. D. 1972 The instability of a vortex sheet on a subsonic stream under acoustic radiation. *Proc. Camb. Phil. Soc.* **72**, 465–488.

JONES, D. S. & MORGAN, J. D. 1974 A linear model of a finite amplitude Helmholtz instability. *Proc. R. Soc. Lond.* A **338**, 17–41.

LEISSA, A. W. 1973 *Vibration of Shells*, chap. 2. NASA SP-288.

MCALPINE, A. & WRIGHT, M. C. M. 2006 Acoustic scattering by a spliced turbofan inlet duct liner at supersonic fan speeds. *J. Sound Vib.* **292**, 911–934.

MORGAN, J. D. 1975 The interaction of sound with a subsonic cylindrical vortex layer. *Proc. R. Soc. Lond.* A **344**, 341–362.

MUNT, R. M. 1977 The interaction of sound with a subsonic jet issuing from a semi-infinite cylindrical pipe. *J. Fluid Mech.* **83**, 609–640.

MYERS, M. K. 1980 On the acoustic boundary condition in the presence of flow. *J. Sound Vib.* **71**, 429–434.

NOBLE, B. 1958 *Methods based on the Wiener–Hopf Technique for the Solution of Partial Differential Equations*. Pergamon.

PAÏDOUSSIS, M. P. 2004 *Fluid-Structure Interactions Vol. 2*. Elsevier.

PEAKE, N. 1997 On the behaviour of a fluid-loaded cylindrical shell with mean flow. *J. Fluid Mech.* **338**, 387–410.

RICHTER, C. & THIELE, F. H. 2007 The stability of time explicit impedance models. *AIAA Paper* 2007-3538.

RIENSTRA, S. W. 2003 A classification of duct modes based on surface waves. *Wave Motion* **37**, 119–135.

RIENSTRA, S. W. 2006 Impedance models in time domain, including the extended Helmholtz resonator model. *AIAA Paper* 2006-2686.

RIENSTRA, S. W. 2007 Acoustic scattering at a hard–soft lining transition in a flow duct. *J. Engng. Maths.* **59**, 451–475.

RUDIN, W. 1991 *Functional Analysis*, p. 380. McGraw-Hill.

TAM, C. K. W. & AURIAULT, L. 1996 Time-domain impedance boundary conditions for computational aeroacoustics. *AIAA J.* **34**, 917–923.

TAM, C. K. W. & JU, H. 2006 Scattering of acoustic duct modes by axial liner splices. *AIAA Paper* 2006-2459.